Highlights of Spanish Astrophysics XI, Proceedings of the XV Scientific Meeting of the Spanish Astronomical Society held on September 4–9, 2022, in La Laguna, Spain. M. Manteiga, L. Bellot, P. Benavidez, A. de Lorenzo-Cáceres, M. A. Fuente, M. J. Martínez, M. Vázquez- Acosta, C. Dafonte (eds.), 2023

Observing black holes with mm-VLBI and the EHT.

Martí-Vidal, I.[1,2]

[1] Dpt. Astronomia i Astrofísica, Universitat de València (Spain)
[2] Observatori Astronòmic, Universitat de València (Spain)

Abstract

The Very Long Baseline Interferometry (VLBI) technique allows us to synthesize virtual telescopes with optical apertures as large as the Earth's diameter (and beyond). With these apertures, when observing at millimeter wavelengths, it is possible to obtain images of the radio universe with a diffraction limit of just a few tens of micro-arcseconds, which is high enough to resolve the "photon rings" of the closest supermassive black holes (SMBH) to the Earth. In these proceedings, we discuss about the challenges of doing VLBI at such short wavelengths and the scientific exploitation of this kind of observations, with an emphasis on the results published by the Event Horizon Telescope (EHT) Collaboration for SgrA* and M87*.

1 Introduction

One of the most exotic predictions of the Theory of General Relativity (GR) is the existence of event horizons in black holes. These are regions where time and space exchange their metric signs, still observers cease to exist as seen from distant reference frames, and two causally-disconnected parts of the Universe meet. The direct observation of black holes at the spatial scales of their event horizons is a way to probe the edge of space and time, which marks the frontier of the Universe that can be accessible to us. Monitoring black holes at these spatial scales may allow, in a longer term, to probe how matter, magnetism, space and time interact and behave in these extreme regions, to test GR (and/or alternative theories of spacetime) in gory detail.

Just a few decades ago, the enterprise of imaging black holes at the scales of their event horizons was in the realm of fiction. The pioneering works of Jean-Pierre Luminet [24] gave us a glance of how these images would look like under ideal conditions, while the more realistic simulations by Heino Falcke [16] demonstrated the feasability of getting observational signatures of the presence of an event horizon (the so-called "black hole shadow") via high-resolution observations at radio wavelengths with the Very Long Baseline Interferometry (VLBI) technique.

The World had to wait many years of technological developments in Radio Astronomy to have stable and sensitive VLBI receivers at millimeter wavelengths; short enough to provide the spatial resolutions needed to image the scales of the event horizons of the closest supermassive black holes (SMBH) to the Earth, specifically those at the center of galaxy M87 (known as M 87*) and our Galactic Center (known as Sgr A*). Here, the critical roles of Shep Doeleman in the american side (Harvard/MIT), and Anton J. Zensus and Thomas Krichbaum in the european side (MPIfR), together with other several pioneers of millimeter-VLBI, cannot be stressed enough.

Two main teams (in California and Europe) were responsible of the development of the first VLBI receivers at 230 GHz (wavelength of 1.3 mm) starting in the 80s−90s decades of the last century, with the first reported VLBI detection at this frequency (actually, at 215 GHz, between the IRAM-30m telescope at Pico Veleta in Spain and the Plateau de Bure interferometer, the current NOEMA, in the french Alps) from year 1995 [20]. The mm-VLBI technology has improved relatively fast since then. In Spain, for instance, the Centro Astronómico de Yebes (CAY), part of the Instituto Geográfico Nacional (IGN), has become a World-leading institution in the development of mm-wave heterodyne receivers.

Shep Doeleman, the founding director of the Event Horizon Telescope (EHT), was the PI of the first VLBI observations of Sgr A* and M 87* at 230 GHz, originally made with just three stations (CARMA in California, SMT in Arizona and JCMT in Hawaii), but good enough to extract some important structural information from the underlying SMBH images (e.g., [4, 5]).

Some years later, with the arrangement of the EHT, new VLBI observations of M 87* and Sgr A* at 230 GHz were finally taken, with an array large and sensitive enough to bring imaging capabilities: the first scientific observations of the modern version of the Event Horizon Telescope took place in April 2017 (see the distribution of EHT stations in Figure 1, left). And, finally, a few years after those observations were taken, the first images of these black holes were revealed to the World by the EHT Collaboration [6, 13].

In the following sections, we will briefly describe how VLBI works and will discuss about the challenges inherent to the mm-wave VLBI observations. Then, we will discuss about the theory behind the images of black holes at the scales of their event horizons, and will briefly summarize some of the main results reported by the EHT Collaboration.

2 Astronomical Interferometry in a nutshell

VLBI is based on the *Aperture Synthesis* technique (e.g., [28]), which enables the combination of a set of small telescopes, in order to "synthesize" a large virtual telescope. Such large synthesized apertures are key to achieve the diffraction-limited high angular resolutions needed to image black holes at the scales of their event horizons (a few tens of μas).

The small telescopes that are combined in the Aperture Synthesis are equiped with heterodyne receivers, which coherently sample different points of the frontwave coming from the observed source. The signals of all these telescopes are recorded and combined (correlated) among all pairs of telescopes, in such a way that it is possible to use all these cross-correlations

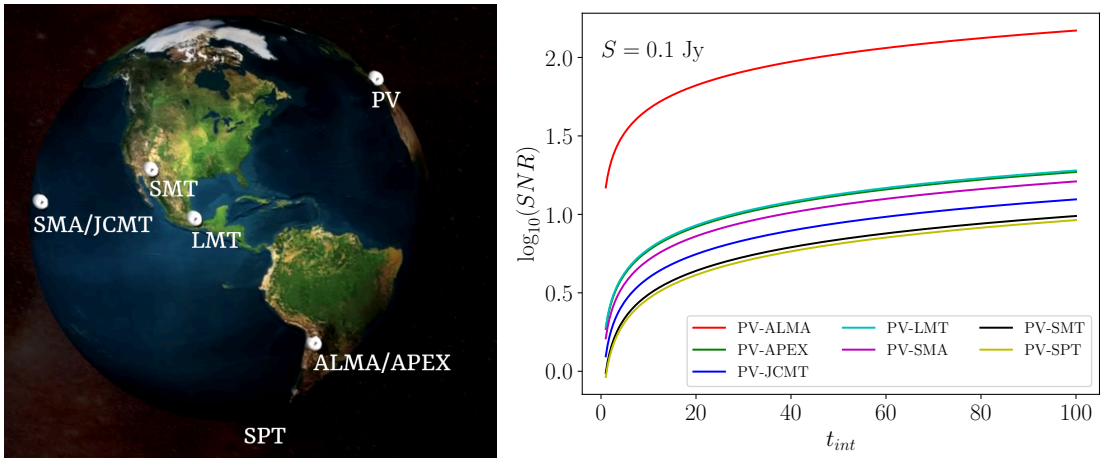

Figure 1: **Left**, array distribution of the EHT in the observing campaign of year 2017. **Right**, theoretical SNR of all the baselines associated to IRAM-30m (PV) in year 2017, assuming a perfect atmosphere and a correlated flux density of 0.1 Jy.

to synthesize the optical aperture of one single "virtual" telescope, with a size equivalent to the maximum distance among the individual elements of the interferometer. The very basic concepts of this technique are sketched in Figure 2. Let us ellaborate on this figure:

In panel **(a)**, we show a set of individual small telescopes (in red) and a giant telescope (in yellow), as large as the space occupied by the set of red telescopes. Panel **(b)** shows the optical aperture (in Fourier space) generated by the interferometer (in red) and the giant telescope (in yellow). For the giant telescope, the aperture is equal to the autocorrelation of its pupile (which we assume to be a perfect circle of size equal to that of the primary reflector surface); for the interferometer, the aperture is determined by the relative positions among all the pairs of telescopes, as seen from the direction to the source. We notice that the interferometer acts like a severe "mask" applied to the whole aperture (since there are only a few points measured in Fourier space!). That mask filters out a large fraction of the spatial frequencies of the observed source structure.

In panel **(c)**, we show the Point Spread Function (PSF, i.e., the instrumental response to a point source) of the giant telescope (i.e., having a full aperture), which is equal to an Airy disc (the sidelobes of the Airy disc are far too weak to be seen with the color palette of this figure). In panel **(d)**, we show (using a similar contrast for the color palette) the PSF corresponding to the sparse aperture of the interferometer, which (due to the large masked regions in Fourier space, see panel **(b)** in red) suffers from relatively large artifacts (i.e., very high sidelobes and secondary peaks). Ellaborated image reconstruction algorithms are needed to get rid of all the convolution artifacts produced by these so-called "dirty" interferometric PSFs (see, e.g. [7, 14]).

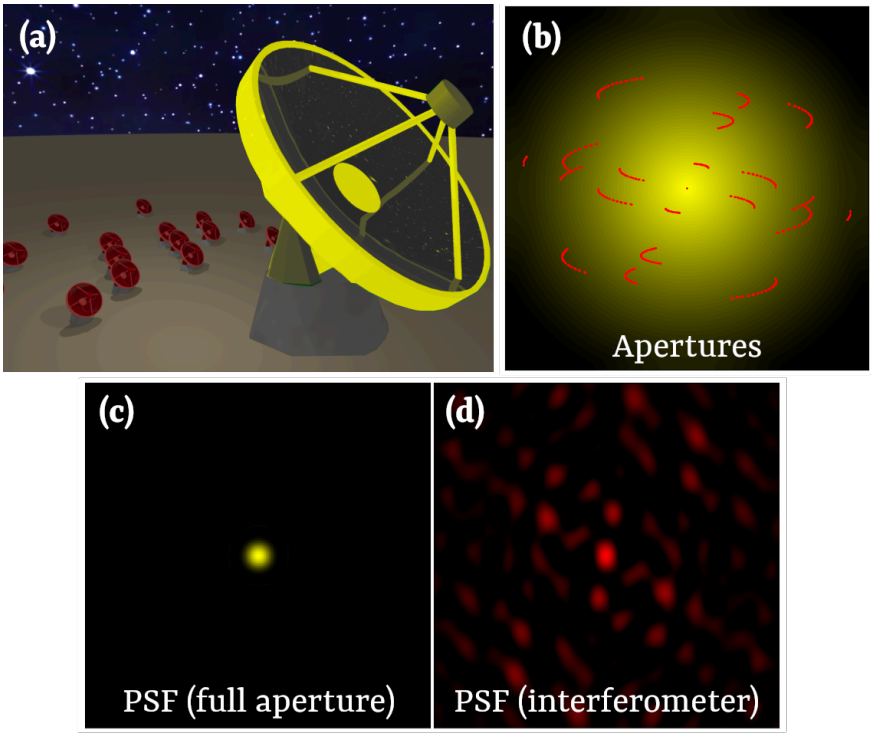

Figure 2: Sketch of how Aperture Synthesis works. **(a)** array distribution (red) and giant telescope with an equivalent resolution (yellow). **(b)** apertures of the interferometer (red) and the giant telescope (yellow). **(c)** and **(d)**, PSFs of the two instruments.

3 The challenge of VLBI at millimeter wavelengths

Observing with VLBI at very high frequencies (millimeter wavelengths) adds some extra problems to the Aperture Synthesis technique described in the previous section. The main problem of mm-VLBI is the relatively low sensitivity of the antenna receivers. It is technically challenging to properly amplify and mix the wideband high-frequency signals, adding a minimum thermal noise across the full signal chain. On the one hand, the reflector surfaces of the antennas have to be built with an extremely high precision (tens of microns), which limits the effective surface of big radiotelescopes. On the other hand, the heterodyne technology at such high frequencies is not very efficient, compared to centimeter wavelengths.

An additional problem (which combines very badly with the first one) is the relatively short coherence time of the atmosphere at these high frequencies[1]. In VLBI, there is a rule of thumb about the coherence time (not very accurate; just valid for order-of-magnitude discussions): for a given observation, *the coherence time in minutes is equivalent to the observing wavelength in centimeters*. That is, for the EHT (observing wavelength of 1 mm)

[1]The coherence time can be defined as the integration time of the interferometric observables, such that the random variations of the atmosphere over each station introduce a loss of 10% in the cross-correlated signal.

the coherence time is of the order of just a few seconds (actually, in [7] there is a more precise estimate of the coherence time of the EHT baselines, which can easily reach more than 20 seconds in most cases).

These two problems combined (i.e., the short coherence time and the limited sensitivity, which implies the need of long integration times to have good detections) prevented the possibility of obtaining VLBI images at 1 mm for many years; until the EHT came online on April 2017. The game changer that allowed to extract the maximum potential of the EHT antennas was the addition of the ALMA telescope to the EHT array (see [18, 26, 25] for details). Figure 1 (right) shows the theoretical SNR of a typical observation (correlated flux density of 100 mJy) for all baselines associated to Pico Veleta (PV), as a function of the integration time (if no atmospheric effects were present). The baseline to ALMA is so sensitive, that there are clear detections after an integration time of just one second (or even a fraction of a second!), which allows to correct for the rapid atmospheric effects, in a way similar to the adaptive optics of optical telescopes. Once these effects are corrected for the whole array (thanks to the baselines to ALMA), much longer integration times can be applied to the whole EHT, ensuring good detections across all the antenna pairs. The interested reader will find more details about the data calibration and analysis in the EHT publications [6, 7].

4 Black hole images at the highest resolutions

What do we see when we observe a black hole with a spatial resolution similar to the size of its event horizon? The first answer to this question came from Jean-Pierre Luminet [24], who realized that the image of the accretion disc could be heavily deformed by the space curvature (the well-known gravitational lensing effect) and, in addition to this, the image of a *ring* would appear around the black hole, as a result of the presence of the so-called *photon sphere* of the black hole. The photon sphere is the region around a black hole where closed photon orbits can exist. Since these orbits are all unstable, photons that orbit arbitrarily close to the photon sphere can eventually escape from that region (after performing a given number of orbits around the black hole) and propagate in direction to the Earth, to be (much) later sampled by the EHT antennas.

The size of the ring associated to the photon sphere encodes precise information about the mass of the black hole, to the point that it can be used either to estimate the mass/distance relation of the black hole, or (if that quantity is already known) to test GR and the spacetime metric of the SMBH.

In Figure 3 (top left), we show an image similar to the results published in [24], where we have used a geometrically thin disc around a Schwarzschild black hole. The inner radius of the disck is set at the innermost stable circular orbit (ISCO). The vertical orange line marks the spin axis of the accretion disc and the dashed blue line marks the edge of the event horizon. The ring image of the photon sphere (about 2.6 times larger than the size of the event horizon) is clearly seen in the image, surrounded (after a small gap) by the image of the accretion disc.

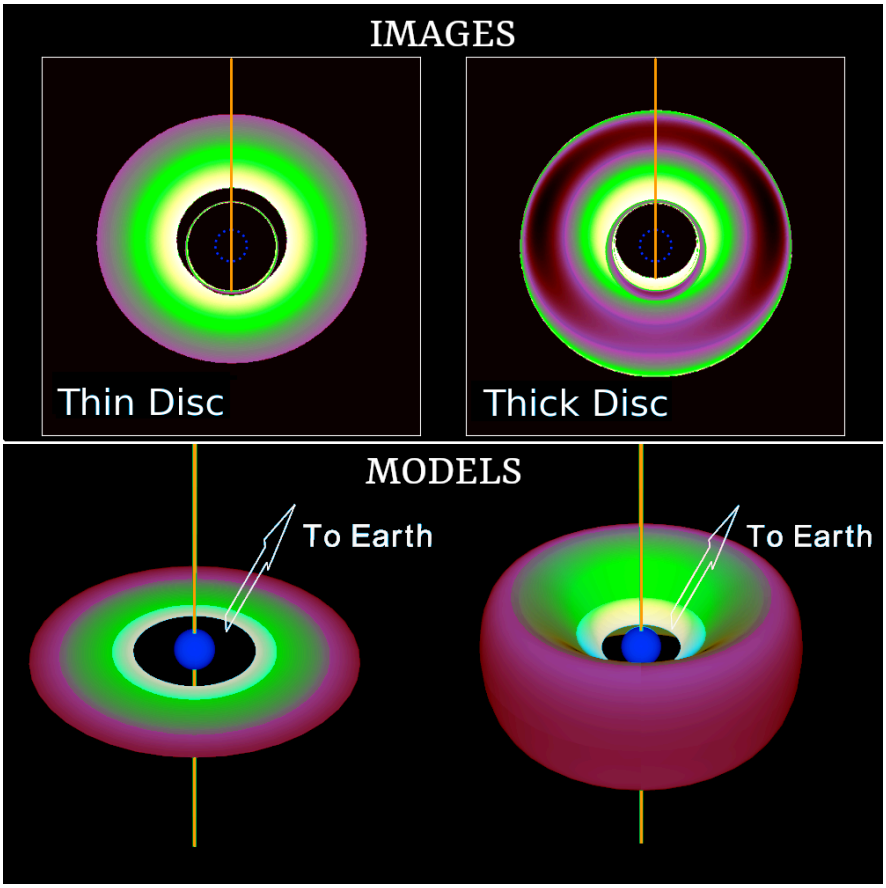

Figure 3: Simulated images of Schwarzschild black holes surrounded by accretion discs. The color palette helps identify the origin of the light rays in the images. **Bottom panels**, disc models used in the simulation; **top panels**, black hole images (Doppler boosting has been disconnected, for clarity). **Left**, the case of a geometrically thin disc; **right**, the case of a geometrically thick (but optically thin) disc. The event horizons are shown as dashed blue lines (top panels) and blue spheres (bottom panels).

However, in real black holes, the accretion discs may not be geometrically thin, especially if the discs are radiatively inneficient (e.g., [27]). These thick geometries add an extra complexity to the images of the black holes, mixing the ring image from the photon sphere with the emission from the disc.

To further complicate this, black holes can also rotate, deforming the photon spheres and the ring images, in ways that depend on the orientation to the observer. In a rotating black hole, there is also an *ergosphere*, where space is being rotationally dragged at superluminal speeds (with respect to distant observers), heavily affecting the dynamics of the accretion and, as a consequence, the black hole images. If the rotation of the black hole is high (Kerr rotation parameter, a, close to unity), the ISCO, the ergosphere, and the photon sphere may even coexist spatially, at similar distances to the black hole. In Figure 4 (left panel) we

show how the size of the ISCO, the ergosphere, and the radii of the photon orbits depend on the black hole rotation (a parameter). Notice that the retrograde (marked as $+$) orbits are always larger than the prograde ones (marked as $-$). The red and blue shaded regions give the range of sizes of the radial photon orbits and "Ergorad" refers to the (equatorial) radius of the ergosphere.

In the same Figure 4 (right panel), we show a representation of the Kerr metric for $a = 0.9$, showing the retrograde (prograde) photon spheres in dark (light) orange, together with some representative photon orbits at those regions (frame-dragging effects, which introduce strong precession in the orbits, are not included, for clarity). The white orbit shown corresponds to the photons with no angular momentum with respect to the rotation axis of the black hole. The ergospheres (outer and inner), the event horizons (outer and inner) and the physical singularity are shown (respectively) in green, red, light grey, dark grey and blue.

When all these effects are properly taken into account, the conclusion is clear: detecting (and measuring the size of) the ring associated to the photon sphere is not an easy task. Strong contamination from the accretion disc must be taken into account, which in turn depends on many unknown parameters: from the amount of rotation of the black hole (and the orientation of the spin axis with respect to the Earth) to the brightness distribution of its accretion disc. In the next sections, we give a very brief description of the strategy followed by the EHT Collaboration to "calibrate" the effect of the accretion disc in the image of M 87* (and Sgr A*).

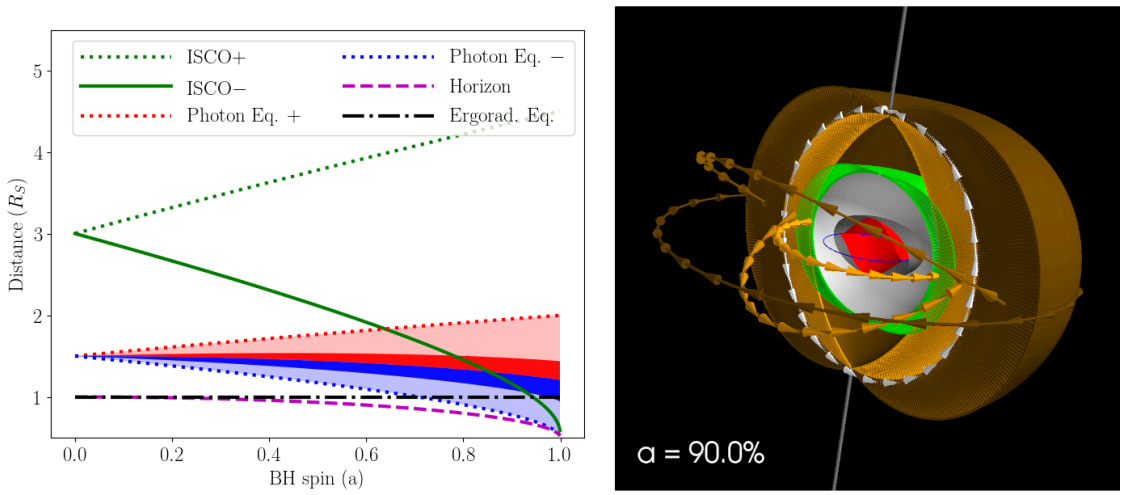

Figure 4: **Left**, size of the ISCO (in green; retrograde $+$ and prograde $-$), photon orbits (red/blue for retrograde/prograde) even horizon (magenta) and ergosphere at the equator (black), as a function of Kerr rotation parameter, a. **Right**, sketch of the phton sphere (retrograde/prograde in dark/light orange) and other peculiar surfaces (see text) for a Kerr black hole with $a = 0.9$.

5 The EHT images of M 87* and Sgr A*

Several active galactic nuclei (AGN) were observed during the EHT campaign of April 2017. Results have been published for some of them (e.g., [23, 22, 21]). In any case, the two most important targets of the whole campaign were M 87* and Sgr A*. The image of M 87* was published about two years after the observations were taken (this gives an idea of the complexity of the calibration and analysis of mm-VLBI data), while it took five years to publish the results on Sgr A* (this gives an idea of the additional complexity in the analysis of this source, for reasons that are discussed in Section 5.2).

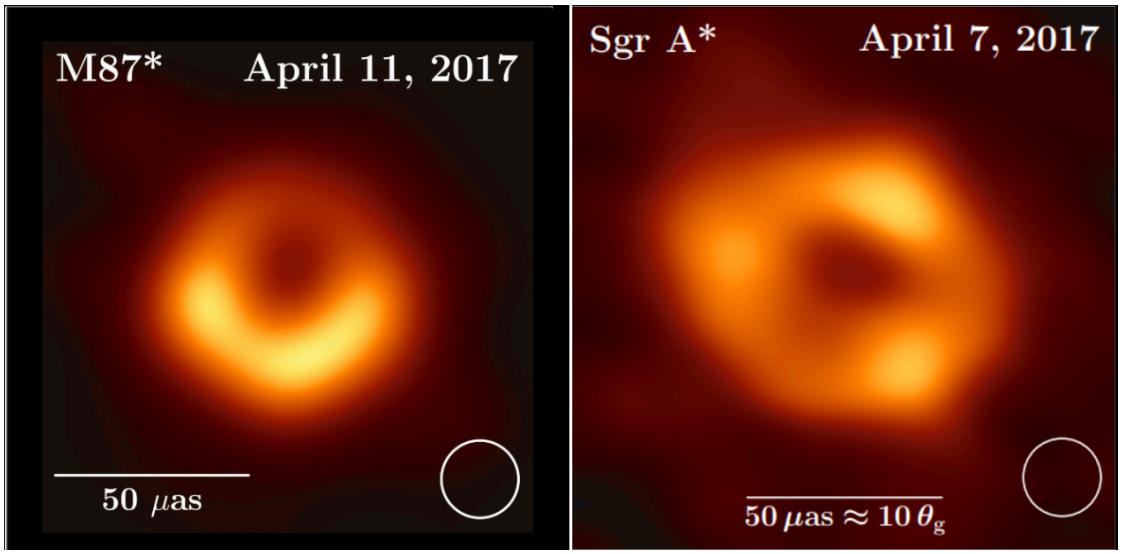

Figure 5: Images of M 87* (left) and Sgr A* (right) published by the EHT Collaboration [6, 13]

5.1 M 87*

The image of M 87* (shown in Figure 5, left) was the first observational confirmation of the *shadow* predicted in [16]. The central brightness depression (the shadow) is surrounded by an assymmetric ring, which is (partially) associated to the photon sphere around the black hole. Actually, only about 10−30% of the brightness in the M 87* image may be related to the photon sphere (e.g., [8, 3]).

By using a large set of realistic simulations of M 87* (with different rotations, orientations, levels of accretion, etc.), the EHT Collaboration estimated the expected range of biases between the size of the observed M 87* image and the size of the underlying photon sphere ring. Adding this "disc contamination" into the analysis and error budget allowed to have a relatively precise estimate of the ring angular size, $\theta_{\rm ring} \sim 42\,\mu$as [8, 9, 10], which in turn could be used to estimate the mass of M 87* (given its known distance), giving the value of $M_{\rm M87*} = (6.5 \pm 0.7) \times 10^9\,{\rm M}_\odot$. This value could then be compared to other independent

estimates, based on either the gas or the stellar bulk dynamics at the central region of the galaxy. The results, which are compatible with the mass estimate of M 87* coming from the stellar dynamics, can be understood as the first confirmation of GR using the most extreme gravitational lensing effect detected to date (i.e., the ring image of a photon sphere).

5.1.1 Polarization: magnetic field and jet launching

Two years after the publication of the M 87* image in total intensity, the EHT Collaboration published its *polarized* version [11, 12], which encodes precise information about the magnetic field geometry at the innermost side of the accretion disc. This information made it possible to constrain the parameter space of the accretion considerably, which also helps to better characterize the "disc contamination" on the estimate of the ring size. These constrains from the polarization also provide valuable information on the physics of accretion and jet launching in M 87*. From the results in [12], the launching of the relativistic jet in M 87* is very likely related to the Blandford-Znajek mechanism [2], where the poloidal component of the magnetic field in the disc, coupled to the presence of an ergosphere, originates an extraction of rotational energy from the black hole by the magnetic field, which is transferred to a plasma propagating along the jet at relativistic speeds. In Figure 6, we show the polarized image of M 87* (corresponding to the observations on April 11, 2017) and a sketch of the magnetic field geometry that could originate the BZ process.

The curly distribution of the polarization angle along the ring (which is represented by the lines of the "wind plot" shown in Figure 6, left) is a combination of the (poloidal dominated) magnetic field in the disc and the light-ray bending due to the space curvature produced by the SMBH.

5.2 SgrA*

Even though the angular scales of the images of M 87* and Sgr A* look similar (see Figure 5), their linear scales are completely different. On the one hand, M 87* is located at a distance of $\sim 16.8^{+0.8}_{-0.7}$ Mpc (e.g., [1]), which translates (for a gravitational size of $\theta_g = 3.8 \pm 0.4\,\mu$as [10]) into a gravitational radius of ∼64 AU. On the other hand, Sgr A* is at a distance of only ~ 8 kpc, which translates (for a gravitational size of $\theta_g = 9.6^{+2.8}_{-1.4}\,\mu$as [15]) into a gravitational radius of ∼0.04 AU (i.e., ∼ 1600 times smaller than M 87*). The dynamical times in both black holes are thus completely different. While in M 87* the dynamical scale is of several days (which means that the image of the ring is not expected to change much during an observation epoch of just several hours), the variability timescale of Sgr A* is just of a few minutes, which means that the image of Sgr A* may change completely, many times, during one single observing epoch of a few hours. In addition to this, the interstellar scattering produced by all the medium of the galactic disc situated between Sgr A* and the Earth, affects the spatial frequencies of the black hole image, which is an effect that also has to be taken into account during the analysis.

One of the basic tenets of the Aperture Synthesis technique is that the source structure should remain stable during the several hours needed to fill (by means of the Earth rotation)

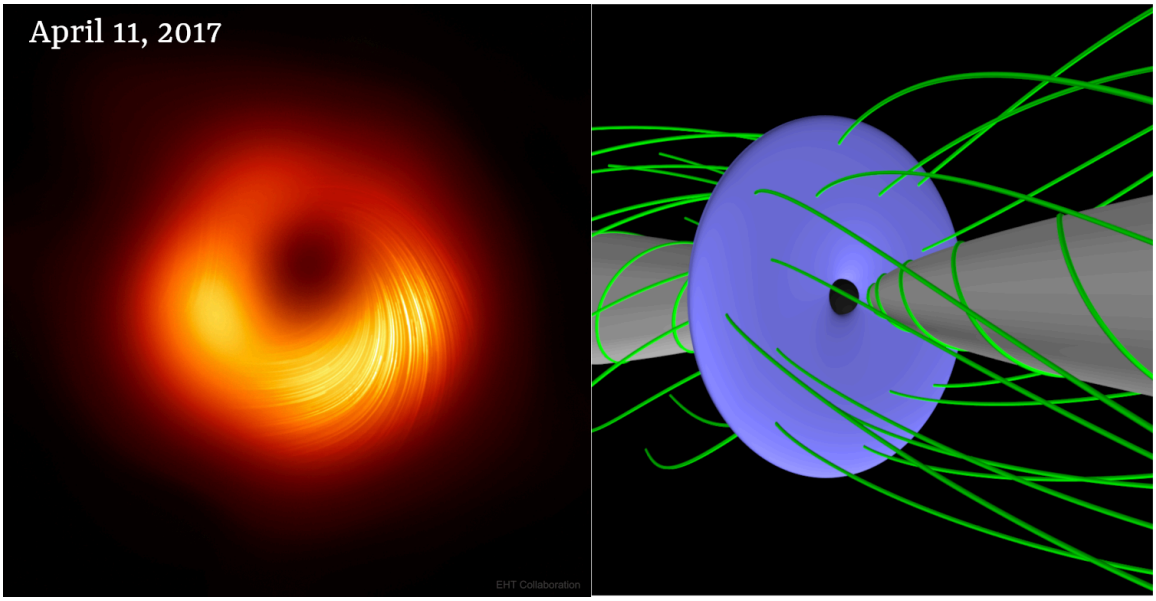

Figure 6: **Left**, "wind plot" version of the polarized image of M 87*, published by the EHT Collaboration in 2021 [11, 12]. **Right**, sketch of an accretion disc with poloidal magnetic field that gets "rolled up" due to the rotation of the central black hole.

the synthesized aperture of the interferometer. Therefore, the rapid variability of the image of Sgr A* required the development of a complete set of new algorithms (as well as a whole suite of simulations and tests) to confidently reconstruct an average image of Sgr A* (e.g., [14]). All these extra works delayed the publication of the long-awaited image of our Galactic Center by several years!

But the prize was worth the long waiting time. The distance to (and the mass of) Sgr A* are known with much higher precision than those of M 87*, thanks to the precision astrometry monitoring works on the Sgr A* field (see [17, 19] and references therein). This means that an estimate of the ring size of Sgr A* can provide more stringent tests of GR than that of M 87*, as well as restrictive tests of alternative spacetime metrics of the black hole. In one of the papers of the EHT Collaboration [15], several of such tests are presented, which combined with those on M 87*, have become a consistent test of GR covering several orders of magnitude in the mass of the black holes.

6 Conclusions

The images of M 87* and Sgr A* published by the EHT Collaboration in 2019 and 2022 represent an inflection point in observational Astrophysics. Before April 2019, the immediate neighbourhood of an event horizon could only be imagined and simulated. Now, thanks to the EHT, it has become routinely possible to observe the innermost side of the accretion discs in SMBH and the regions where light is bent in orbits around the edge of space and time.

And this is just the beginning for the EHT. The images shown in Figure 5 are the first frames of a great movie that now starts to be recorded; a movie where we will see how black holes feed and produce their relativistic jets, one of the most energetic and misterious phenomena in the Universe.

Acknowledgments

This work has been partialy supported by the GenT program of Generalitat Valenciana (Project CIDEGENT/2018/021) and by MICINN Project PID2019-108995GB-C22.

References

[1] Bird, S., Harris, W. E., Blakeslee, J. P. & Flynn, C. 2010, A&A, 524, 71

[2] Blandford, R. D. & Znajek, R. L. 1977, MNRAS, 179, 433

[3] Broderick, A. E., Pesce, D. W., Gold, R., et al. 2022, ApJ, 935, 61

[4] Doeleman, S. S., Fish, V. L., Schenck, D. E., et al. 2012, Science, 338, 6105, 355

[5] Doeleman, S. S., Weintroub, J., Rogers, A. E. E., et al. 2008, Nature, 455, 7209, 78

[6] EHT Collaboration 2019, ApJL, 875, 1

[7] EHT Collaboration 2019, ApJL, 875, 3

[8] EHT Collaboration 2019, ApJL, 875, 4

[9] EHT Collaboration 2019, ApJL, 875, 5

[10] EHT Collaboration 2019, ApJL, 875, 1

[11] EHT Collaboration 2021, ApJL, 910, 12

[12] EHT Collaboration 2021, ApJL, 910, 13

[13] EHT Collaboration 2022, ApJL, 930, 12

[14] EHT Collaboration 2022, ApJL, 930, 14

[15] EHT Collaboration 2022, ApJL, 930, 17

[16] Falcke, H., Melia, F. & Agol, E. ApJL, 528, 13

[17] Ghez, A. M., Salim, S., Weinberg, N. N., et al. 2008, ApJ, 689, 2

[18] Goddi, C., Crew, G. B., Impellizzeri, V., et al. 2019, The Messenger, 177, 25

[19] GRAVITY Collaboration 2018, A&A, 618, L10

[20] Greve, A., Torres, M., Wink, J. E., et al. 1995, A&A, 299, L33

[21] Issaoun, S., Wielgus, M., Jorstad, S., et al. 2022, ApJ, 934, 145

[22] Janssen, M., Falcke, H., Kadler, M., et al. 2021, Nature Astronomy, 5, 1017

[23] Kim, J-Y., Krichbaum, T. P., Broderick, A. E., et al. 2020, A&A, 640, 69

[24] Luminet, J.-P. 1979, A&A, 75, 228

[25] Martí-Vidal, I., Roy, A., Conway, J. & Zensus, A.$\frac{1}{2}$J. 2016, A&A, 587, 143

[26] Matthews, L. D., Crew, G. B., Doeleman, S. S., et al. 2018, PASP, 130, 983

[27] Narayan, R., Sadowski, A., Penna, R. F. & Kulkarni, A. K. 2012, MNRAS, 426, 3241

[28] Thompson, A. R., Moran, J. M. & Swenson, G. W. 2017, *Interferometry and Synthesis in Radio Astronomy*, Springer (3rd edition)